

This is the peer reviewed version of the following article:

Optical properties of the dibenzothiazolylphenol molecular crystals through ONIOM calculations: the effect of the electrostatic embedding scheme / Presti, Davide; Pedone, Alfonso; Ciofini, Ilaria; Labat, Frédéric; Menziani, Maria Cristina; Adamo, Carlo. - In: THEORETICAL CHEMISTRY ACCOUNTS. - ISSN 1432-881X. - ELETTRONICO. - 135:4(2016), pp. 1-11. [10.1007/s00214-016-1808-x]

*Terms of use:*

The terms and conditions for the reuse of this version of the manuscript are specified in the publishing policy. For all terms of use and more information see the publisher's website.

18/11/2024 19:20

(Article begins on next page)

[Click here to view linked References](#)

1  
2  
3  
4 **Optical properties of the dibenzothiazolyphenol molecular crystals**  
5  
6  
7  
8 **through ONIOM calculations: the effect of the electrostatic**  
9  
10  
11 **embedding scheme.**  
12

13 Davide Presti<sup>1,\*</sup>, Alfonso Pedone<sup>1</sup>, Ilaria Ciofini<sup>2</sup>, Frédéric Labat<sup>2</sup>, Maria Cristina Menziani<sup>1</sup> and

14  
15  
16 Carlo Adamo<sup>2,3</sup>  
17

18  
19 <sup>1</sup>*Dipartimento di Scienze Chimiche e Geologiche, Università di Modena e Reggio-Emilia, via G.*  
20 *Campi 103, I-41125 Modena, Italy.*  
21

22 <sup>2</sup>*Institut de Recherche de Chimie Paris CNRS Chimie ParisTech, 11 rue P. et M. Curie, F-75005*  
23 *Paris 05, France.*  
24

25  
26 <sup>3</sup>*Institut Universitaire de France, 103 Boulevard Saint Michel, F-75005 Paris, France.*  
27  
28  
29  
30  
31  
32  
33  
34  
35  
36  
37  
38  
39  
40

41 **Corresponding Author**  
42

43  
44 Dr. Davide Presti,

45  
46 Department of Chemical and Geological Sciences,

47  
48 University of Modena and Reggio Emilia, via G. Campi 103, Modena, 41125, Italy.  
49

50  
51 E-mail: [davide.presti@unimore.it](mailto:davide.presti@unimore.it);  
52  
53  
54  
55  
56  
57  
58  
59  
60  
61  
62  
63  
64  
65

1  
2  
3  
4 **Abstract**  
5

6 Periodic Density Functional Theory and hybrid ONIOM time-dependent DFT/MM cluster  
7  
8 calculations have been carried out to investigate the ground and excited state properties of the  
9  
10 crystalline structures of the enolic and ketonic tautomeric forms of a propoxy-substituted  
11  
12 dibenzothiazolylphenol molecule (**OPr**), a prototype for systems undergoing to the excited state  
13  
14 intramolecular proton transfer process.  
15  
16

17  
18 The crystalline structures of the tautomeric forms are well reproduced and, as expected, at the  
19  
20 ground state the enol polymorph is predicted to be more stable than the keto one. At the excited  
21  
22 state, the effect of the environment on time-dependent DFT calculations has been accounted for  
23  
24 by including a charge embedding scheme, and the influence of different kinds of point charges  
25  
26 (Mulliken, CM5, RESP and  $Q_{Eq}$ ) in determining the optical properties of the central molecule has  
27  
28  
29 been investigated.  
30  
31

32  
33 The results reveal that, in fair agreement with experimental data, the absorption (emission)  
34  
35 energies of the enol (keto) **OPr** molecule is red shifted of about 3 (3) nm going from the gas  
36  
37 phase to chloroform and blue shifted of 10 (23) nm going from the gas to the crystal phase when  
38  
39 the electronic embedding with Mulliken charges is employed. The electrostatic embedding  
40  
41 influence the excited state properties more severely than the ground state and, apart the  $Q_{Eq}$   
42  
43 charges, all other models provide Stokes' shifts in reasonable agreement with experimental data.  
44  
45  
46  
47

48  
49 **Keywords** : ES IPT fluorophores, molecular crystals, TD-DFT, ONIOM, electrostatic embedding  
50  
51  
52  
53  
54  
55  
56  
57  
58  
59  
60  
61  
62  
63  
64  
65

## 1. Introduction

In the last years, molecular solids have found a large growth in applications as optic materials with versatile uses in photochemical science and engineering.[1]

Several organic molecules exhibiting *charge transfer* (CT) and/or Excite-State Intramolecular Proton Transfer (ESIPT) processes after irradiation have shown interesting photo-chromic properties when arranged in the solid state.[2–5]

Recently, Sakai et al.[6] synthesized and characterized (by X-Ray Diffraction and UV-Visible absorption and fluorescence spectroscopy) four different alcoxy-substituted (methoxy-, ethoxy-, propoxy- and butoxy-) dibenzothiazolylphenol molecular crystals that exhibit strong ESIPT fluorescence.

**Figure 1** reports the chemical structures of the enolic and ketonic forms of the propoxy-substituted compound (hereafter named **OPr**) as well as the photochemical mechanism responsible of its luminescent properties.

This chromic compound shows, both in solution (chloroform solvent) and in solid-state, an orange-red fluorescent emission, that in the crystal gives rise to a remarkable fluorescent quantum yield ( $\Phi_{\text{FL}} = 0.38$ ). The proposed photophysical molecular mechanism involves: i) the photoirradiation of the enol tautomeric form of **OPr**, followed by ii) an ESIPT process that leads to the fluorescent keto tautomer. The spectral differences observed in solid-state fluorescence (not sizeable in the molecular case) for diverse substitutions of the alcoxy- group were explained[6] making use of the Davydov exciton coupling theory.[7] Two systems (**OPr** and the methoxy-substituted one, **OMe**) form H-aggregates, whereas the other two systems (propoxy- and butoxy-substituted) form J-aggregates. The stacked molecular displacement of molecules within the crystal, originates a face-to-face (head to tail) coulomb interaction between the molecular transition dipole moments that for H-aggregates (J-aggregates) yields to a bathochromic

1  
2  
3  
4 (hypsochromic) shifted emission with respect to the non-substituted compound. Therefore, the  
5  
6 emissive lowest singlet excited state is destabilized (overstabilized) depending on the competing  
7  
8 dipole-dipole interactions.  
9

10  
11 Such experimental observations were partially supported[6] only for **OMe**, with a Density  
12  
13 Functional Theory (DFT) computation in gas-phase of HOMO-LUMO frontier orbitals of the two  
14  
15 tautomers at the ground state geometry. These calculations, however, did not provide much  
16  
17 theoretical information on the optical properties of **OMe** and, more in general, on this family of  
18  
19 red fluorophores, since excited states were not examined. Moreover, environmental effects  
20  
21 mimicking the solvent (chloroform) and/or the solid material were not considered.  
22  
23

24  
25 The aim of the present work is to provide theoretical insights into the chromic properties of such  
26  
27 family of solid compounds through the study of the **OPr** system (for which the experimental enol  
28  
29 structure is available), utilizing a computational protocol based on a quantum mechanical (QM)  
30  
31 periodic approach coupled with ONIOM QM/MM cluster calculations.[8] The results obtained  
32  
33 will allow the assessment of the efficiency of such protocols for ES IPT molecular crystalline  
34  
35 materials as **OPr**, and the derivation of useful indications for future theoretical modelling of solid  
36  
37 state fluorophores.  
38  
39

40  
41 In fact, although the photophysical/photochemical properties of molecular crystals attracted a  
42  
43 great interest,[9–11] their computational characterization is still in a germinal stage. This is  
44  
45 mainly due to the cost/accuracy ratio of time-dependent techniques needed for the study of very  
46  
47 large systems. Moreover, the complexity of molecular phenomena of interest are unavoidably  
48  
49 combined with the notorious lacks of standard quantum methods (e.g. DFT) in describing non-  
50  
51 classical long-range effects implicitly.[12–14] These lacks, in DFT, have partly been solved with  
52  
53 the introduction of the *a posteriori* correction schemes to recover dispersive interactions.[14]  
54  
55  
56  
57  
58  
59  
60  
61  
62  
63  
64  
65

1  
2  
3  
4 In order to define a feasible approach for describing large solid systems, i.e. a good ratio between  
5  
6 computational cost and accuracy, Density Functional Theory – coupled with the *a posteriori*  
7  
8 dispersion correction[15, 16] – has been adopted to model the crystalline ground-state structures.  
9  
10 Linear response (LR) time-dependent DFT (TD-DFT), within the frame of multiscale ONIOM  
11  
12 QM/MM cluster calculations, has been chosen to investigate the UV-Visible absorption and  
13  
14 emission optical properties from the excited states of **OPr**, and the results have been compared  
15  
16 with standard TD computations on gas-phase and solvated monomers.  
17  
18

19  
20 Finally, since the effect of the environment during the TD-DFT calculations have been accounted  
21  
22 for by using the ONIOM approach,[17, 18] we have investigated the influence of different kinds  
23  
24 of point charges (to describe the low level region) in determining the optical properties of the  
25  
26 central molecule.  
27  
28

29  
30 The paper is organized as follows: computational details are given in Section 2; ground-state  
31  
32 structural properties of the system are commented in Section 3.1, whereas inter- and  
33  
34 intramolecular parameters are discussed in Sections 3.2 and 3.3. The main results on the UV-  
35  
36 Visible optical properties of **OPr** are exposed and commented in Section 3.4. The role played by  
37  
38 charge embedding in this context is analyzed in Section 3.5. Then some general conclusions and  
39  
40 future directions are drawn.  
41  
42  
43  
44  
45  
46

## 47 **2. Computational Details**

48  
49 *2.1 Ground state periodic calculations.* Full structural relaxations of the ground state forms of the  
50  
51 enol- and keto- polymorphs of **OPr**[6] were carried out at the B3LYP-D\*/6-31G(d,p) level[16,  
52  
53 19] using a parallel version of the CRYSTAL09[20, 21] suite of programs. This setting has  
54  
55 proved quite accurate in describing the structural properties of molecular crystals.[22, 23]  
56  
57  
58  
59  
60  
61  
62  
63  
64  
65

1  
2  
3  
4 The performance of the 6-31G(d,p) basis-set was checked against richer basis-sets including  
5  
6 diffuse functions (6-31+G(d,p), 6-311+G(d,p))[24, 25]. The results, which are reported in the  
7  
8 Supporting Information, revealed that the addition of both  $\zeta$ -valence and diffuse functions affects  
9  
10 negligibly the ground state structures.  
11  
12

13  
14 A full use of symmetry and periodic boundary conditions (PBC) was imposed, as implemented in  
15  
16 CRYSTAL09. The Monkhorst-Pack grid was set to 4 4 (see keyword SHRINK),[21] that in the  
17  
18 case of **OPr** corresponds to 30  $k$ -points within the Irreducible Brillouin's Zone. The eigenvalues  
19  
20 level shift was locked to 1 a.u. (LEVSHIFT 10 1), and the thresholds on the convergence of  
21  
22 bielectronic integrals tightened (TOLINTEG 7 7 7 9 18) with respect to default values.  
23  
24

25  
26 The starting structure of the enol form of **OPr** is the one experimentally resolved by Sakai et  
27  
28 al.[6] The structure of the metastable keto polymorph is not known but the same crystal  
29  
30 symmetry of the enol form ( $P2_1/c$  space group) was imposed. Therefore, we manually moved the  
31  
32 hydrogen involved in the ESIPT process from oxygen to nitrogen and optimized the keto form  
33  
34 obtained, keeping the same computational conditions as for the enol polymorph (only the  $\alpha$  and  $\gamma$   
35  
36 parameters were constrained at 90). As a structural check, a symmetry operator search with a  
37  
38 tolerance of 0.01 Å (making use of Accelrys Materials Studio Visualizer, ver. 6.0) on the  $PI$  cell  
39  
40 of the optimized keto polymorph revealed that the crystal maintained the same symmetry. This is  
41  
42 probably the consequence of the large size of the **OPr** molecules, which with their quasi-planar  
43  
44 geometry and the presence of  $\pi$ -stacking interactions and the consequent crystal packing (see  
45  
46 **Figures 2 and 3**), impede possible rotations and other structural changes.  
47  
48  
49  
50  
51

52  
53  
54  
55 **2.2 Monomer calculations.** The ground state of the molecular enol- and keto- forms of **OPr** were  
56  
57 optimized employing the B3LYP[19] density functional approximation.  
58  
59  
60  
61  
62  
63  
64  
65

1  
2  
3  
4 Calculations were carried out in gas-phase and in solution: according to the experimental  
5  
6 measurements carried out in chloroform (CHCl<sub>3</sub>), a Conductor-like Polarizable Continuum  
7  
8 implicit model of solvation[26] (C-PCM) was used to describe CHCl<sub>3</sub>.  
9

10  
11 Excited state properties were computed at the same level of theory as for ground-state, adopting  
12  
13 the 6-31+G(d,p) basis-set. The addition of diffuse functions was necessary for a better description  
14  
15 of the excited-states. As mentioned before, these are not crucial for the structural properties in the  
16  
17 ground state: in the latter case the 6-31G(d,p) basis-set was used also for monomers, for  
18  
19 coherence with PBC calculations.  
20  
21

22  
23 Vertical excitation energies (UV-Visible absorption) were calculated both for the enol and keto  
24  
25 forms (the first ten states have been considered), whereas the full optimization of the first excited  
26  
27 singlet, S<sub>1</sub> (UV-Visible emission), was performed only for the keto form, since this latter is the  
28  
29 responsible for the main fluorescent emission of **OPr** both in solution and in solid-state. All  
30  
31 calculations on monomers and clusters (except for charge embedding, *vide infra*) were carried out  
32  
33 with the Gaussian09 (Rev. D.01) program package.[27]  
34  
35  
36

37  
38 *2.3 QM/QM' cluster calculations.* Inspired by a theoretical protocol discussed elsewhere,[8] to  
39  
40 mimic and predict the photophysical features of **OPr** in solid-state we extracted, from the fully  
41  
42 optimized enol and keto crystalline structures, two clusters of molecules that in the following will  
43  
44 be referred to as **C-OPr-enol** and **C-OPr-keto**, respectively. These both contain 17 **OPr**  
45  
46 molecules (799 atoms, 47 atoms/molecule) in their enol (keto) form. The size of clusters was  
47  
48 chosen in order to include explicitly a surrounding molecular environment of 16 molecules/752  
49  
50 atoms (set as low-level region), i.e. a “cage” that is responsible of the main noncovalent  
51  
52 interactions affecting the central molecule of **OPr** (set as high-level region).  
53  
54  
55

56  
57 Then, the central **OPr** molecule (i.e. the high-level region) of **C-OPr-enol** and **C-OPr-keto** was  
58  
59 further optimized without symmetry constraints, within an ONIOM-like[17, 18] QM/QM' cluster  
60  
61  
62  
63  
64  
65



1  
2  
3  
4 approach in the framework of mechanical embedding. The B3LYP/6-31G(d,p) level of theory  
5  
6 was employed for the QM region, while the Hartree-Fock (HF)/STO-3G method was employed  
7  
8 for the QM' region, whose geometry was maintained fixed at its crystalline structure.  
9

10  
11 Excited state properties (vertical UV-Visible absorption and emission) have been computed at the  
12  
13 QM/QM' level with the same methods. The 6-31+G(d,p) basis-set was used for the high-level  
14  
15 QM region. The fluorescence properties were obtained by optimizing the first bright excited state  
16  
17 ( $S_1$ , singlet), keeping the central molecule of the keto form of **OPr** spatially unconstrained within  
18  
19 the fixed environment region.  
20  
21

22  
23 The simulated UV-Visible spectra were plotted through an in-house code as gaussian  
24  
25 convolutions of the computed main vertical transitions, using a full-width at half maximum  
26  
27 (FWHM) of 0.1 eV. Intensities were normalized to 1 a.u.  
28  
29  
30

31  
32  
33 *2.4 Charge model effects on cluster calculations results.* The effect of the charge model on the  
34  
35 UV-Visible optical properties of clusters were studied by means of TD-DFT/MM single-point  
36  
37 energy calculations coupled with an electrostatic embedding (EE) scheme (involving explicit  
38  
39 charges for the low level system) applied to the ground and excited geometries of the **OPr** central  
40  
41 molecule optimized at the B3LYP/HF level with mechanical embedding.  
42  
43

44  
45 The calculations were carried out by using ground state charges for the low level region. The  
46  
47 Mulliken,[28] CM5,[29] RESP,[30][31] and  $Q_{Eq}$ [32] charges were tested. The Mulliken charges  
48  
49 have been computed at the HF level by using the STO-3G basis set, since it has been  
50  
51 demonstrated to provide good charges (even if for error cancellation).[33]  
52  
53

54  
55 CM5 type charges were computed at the HF/6-31G(d) level and RESP charges were computed at  
56  
57 the HF/STO-3G and HF/6-31G(d).  
58  
59  
60  
61  
62  
63  
64  
65

1  
2  
3  
4 Frontier orbitals were depicted with an isosurface density value of 0.02 a.u. for **OPr** in gas-phase,  
5  
6 solution and (for the central molecules of) cluster systems.  
7  
8  
9

### 10 11 **3. Results and Discussion**

12  
13 *3.1. Ground state polymorphs.* The stable crystalline enol polymorph of **OPr** is characterized by  
14 the presence of 4 molecules ( $Z=4$ ) within the unit cell (188 atoms/cell), that belongs to the  $P2_1/c$   
15 monoclinic space group. The B3LYP-D\*/6-31G(d) fully optimized (atomic positions and lattice  
16 parameters) structure is pictorially represented in **Figure 2**, and compared with the fully  
17 optimized keto structure (additional images of the unit cell are reported in the Supporting  
18 Information). It can be noted that the two polymorphs are very similar, because of the same  
19 crystalline symmetry. The keto form, however, is slightly more closely packed than the enol one,  
20 as confirmed by the differences in cell parameters, reported in **Table 1**.  
21  
22

23  
24 As regards the prediction of cell parameters with respect to experiment (enol form), small  
25 deviations are furnished by B3LYP-D\* (**Table 1**), except for the angle  $\beta$  ( $-1.676^\circ$ ) that is more  
26 severely underestimated. This is probably due to the presence of dispersive interactions  
27 originated by  $\pi$ - $\pi$  stacking patterns between molecules, located along a diagonal vector in the  $ac$   
28 plane. However, the total Relative Deviation % on the unit cell volume (RD %, obtained as  
29  $[\text{Volume}(\text{calc.}) - \text{Volume}(\text{exp.})] / \text{Volume}(\text{exp.}) \times 100$ ) is smaller than 5% ( $-4.40\%$ ). It has to be  
30 recalled, however, that cell volumes are only qualitatively comparable due to thermal effects, the  
31 experimental enol structure being determined at 100 K.  
32

33  
34 As for the keto polymorph, the RD % on volume amounts at  $-0.86\%$ , the major contributions to  
35 this deviation being the shortening of the lattice constant  $b$  ( $-0.170 \text{ \AA}$ ) and the shrinking of the  
36 angle  $\beta$  ( $-0.576^\circ$ ).  
37  
38  
39  
40  
41  
42  
43  
44  
45  
46  
47  
48  
49  
50  
51  
52

1  
2  
3  
4 **Table 1** also reports the theoretical relative stability, obtained as difference between the keto and  
5  
6 enol total ground state energies. As expected, the fully optimized enol polymorph is predicted to  
7  
8 be more stable than the fully optimized keto one, of about 19 kcal/mol. The difference per  
9  
10 molecule (ca. 5 kcal/mol) is larger than what can be expected (1-2 kcal/mol) for crystalline  
11  
12 phases owing such structural similarity. Nonetheless, one should remember that the hydrogen  
13  
14 atom involved in the ES IPT undergoes to a notable displacement from the enol to the keto form  
15  
16  
17  
18 (see below, Section 3.2).  
19  
20  
21  
22

23  
24 *3.2. Crystals vs. Clusters: intermolecular interactions.* The **C-OPr-enol** and **C-OPr-keto** clusters  
25  
26 were extracted from the fully optimized crystals, as described in Section 2.4. We recall that the  
27  
28 B3LYP was employed for the subsequent ground state optimization of the central enol/keto  
29  
30 molecule of **OPr** (high-level region) within the fixed environment of 16 surrounding molecules  
31  
32 (low-level region) treated with HF/STO-3G.  
33  
34

35  
36 As first step in the comparison between crystalline and cluster forms of **OPr**, *intermolecular*  
37  
38 distances have been considered. Selected parameters (among all possible ones included within a  
39  
40 range of 4 Å around the central molecule) are listed in **Table 2**, and shown in **Figure 3** (bottom),  
41  
42 together with atom labels, for the enol tautomer (see Figure S.2 of the Supporting Information for  
43  
44 the keto tautomer).  
45  
46

47  
48 It should be noticed that the distances C16···H(a') and H(a)···C16 are equivalent by symmetry,  
49  
50 as proven by their equal values observed in solid-state (2.735 Å enol form; 3.586 Å keto form).  
51  
52

53  
54 When the central molecule is optimized within a fixed environment such symmetry is broken,  
55  
56 therefore for clusters, the two distances are not equivalent. In particular, the optimized  
57  
58 configuration of **C-OPr-enol** leads to a very small deviation for C16···H(a') (+0.008 Å), while  
59  
60 H(a)···C16 remains the same (3.586 Å). For **C-OPr-keto**, instead, a larger deviation is observed  
61  
62  
63  
64  
65

1  
2  
3  
4 for C16...H(a') (-0.044 Å); a small one is obtained for H(a)...C16 (+0.008 Å). For the other  
5  
6 distances, absolute deviations within 0.0058 Å are given, the larger ones involving hydrogen  
7  
8 atoms. Instead, the measured  $\pi$ - $\pi$  stacking distance remains very similar for the two tautomers, in  
9  
10 solid state and clusters (ca. 3.650 Å). This is ascribable to the fact that molecular flexibility is  
11  
12 impeded by the packing of central **OPr** within its environment.  
13  
14

15  
16 *3.3. Intramolecular parameters: crystals, clusters and monomers.* The comparison between **OPr**  
17  
18 structures in different states of aggregation is important for a better understanding of the optical  
19  
20 properties analyzed in the next Sections. In this case, only *intramolecular* parameters can be  
21  
22 compared. These, however, in both crystals and clusters also reflect the spatial displacements due  
23  
24 to intermolecular interactions. In principle, one should expect some relevant differences between  
25  
26 structures, because monomers in gas phase and in solution have a major number of degrees of  
27  
28 freedom. In crystals, instead, covalent and noncovalent parameters are deeply interdependent, but  
29  
30 constrained to the whole crystal symmetry. Finally, clusters depend on their starting crystalline  
31  
32 geometry, at which the external molecules are fixed; the central **OPr** molecule, nonetheless,  
33  
34 experiences some degree of motion, which is mechanically limited by its inclusion in the  
35  
36 environment.  
37  
38  
39  
40  
41  
42

43  
44 Probably, as a consequence of the mild changes of the intermolecular parameters discussed  
45  
46 above, also the intramolecular ones – a subset of those given in Table S.1 is reported in Table S.2  
47  
48 of the Supporting Information, for the enol tautomer – do not present severe variations between  
49  
50 the different states of aggregation of **OPr**. This is true also when comparing the gas-phase  
51  
52 monomer with the corresponding crystal polymorph: in fact, the gas-phase **OPr** molecule  
53  
54 presents a planar conformation, for which rotations of dihedral angles are negligible – and thus  
55  
56 not reported. As expected, the parameters which show more substantial variations correspond to  
57  
58  
59  
60  
61  
62  
63  
64  
65

1  
2  
3  
4 those related to the intramolecular hydrogen bond (see deviations of O1–H 0.16/0.18 Å; and  
5  
6 H···N1 -0.14/-0.18 Å in Table S.2), especially the angle O1–H–N1 (-4.1° optimized crystal to -  
7  
8 5.7° gas-phase). Nonetheless, this parameter is exposed to marked variations for negligible  
9  
10 changes in the displacement of the hydrogen atom.  
11  
12

13  
14 An interesting aspect is the difference between the ground state optimized geometry ( $S_0$ ) of the  
15  
16 keto tautomer and its excited singlet state ( $S_1$ ) optimized geometry, the latter corresponding to the  
17  
18 optical fluorescent moiety. The related inter- and intra- molecular parameters are compared in  
19  
20 **Table 3**, and the difference between distances of selected intra- and intermolecular parameters  
21  
22 for the **OPr** keto tautomer are given in **Figure 4**.  
23  
24

25  
26 Importantly, the structural variation between  $S_1$  and  $S_0$  have similar extent, and the same sign  
27  
28 independently from the system considered. Looking at H-bond parameters, it is reasonable to  
29  
30 suppose that the ESIPT mechanism, which is nonetheless of intramolecular nature, is actually  
31  
32 transferable from the singly molecular (gas- or solvated-) phase to the (cluster representation of  
33  
34 the) solid-state, at least from a purely structural point of view.  
35  
36

37  
38 **Figure 4** shows that the distances related to the H-bond present larger variations when going  
39  
40 from  $S_1$  to  $S_0$  (ex.: N1···O1 +0.11/+0.12 Å and O1···H +0.21/+0.22 Å), highlighting the rise of a  
41  
42 mild repulsion between the H-bond acceptor species (O1) and both the donor species (N1) and  
43  
44 the H atom. This could represent a stabilization of the keto-imine group, going towards the  
45  
46 excited  $S_1$  minimum from the vertically excited  $S_0$  geometry. The covalent H–N1 bond, instead,  
47  
48 remains almost unaltered (deviation -0.03 Å).  
49  
50

51  
52 Differences in the intermolecular parameters defined before for the enol form (see **Figure 3**), are  
53  
54 reported for the **C-OPr-keto** cluster. All such differences are extremely tiny, falling all within  
55  
56 0.08 Å. The larger ones involve the intermolecular O1···H(c) and O2···H(d) distances (of -0.057  
57  
58 Å and +0.056 Å, respectively).  
59  
60  
61  
62  
63  
64  
65

1  
2  
3  
4  
5  
6 *3.4 Optical properties: gas, solution and clusters.* The vertical excitation and emission energies  
7  
8 of **OPr** molecule in the gas phase, in chloroform and in the crystal are summarized in **Table 4**.

9  
10 **Figure 5** reports both the absorption and the emission spectra obtained from the computed main  
11  
12 TD-B3LYP/6-31+G(d) vertical transitions of gas-phase, solvent (CHCl<sub>3</sub>) and cluster (TD-  
13  
14 B3LYP/6-31+G(d):MM with embedding of HF/STO-3G Mulliken charges). We recall that the  
15  
16 emission spectrum was calculated only for the keto tautomer, since it is the fluorescent system.  
17  
18 The absorption spectrum, on the other hand, corresponds to the enol tautomer, the most stable  
19  
20 form at the ground state.  
21  
22

23  
24  
25 The results reveal that the vertical excitation energy (VEE) of the enol form of **OPr** is red shifted  
26  
27 of about 3 nm going from the gas phase to chloroform and blue shifted of 10 nm when going  
28  
29 from the gas phase to the crystal phase here simulated by the cluster with electronic embedding  
30  
31 using Mulliken charges.  
32  
33

34  
35 The same behavior is observed for the emission energy, that is, the emission of **OPr** in solution is  
36  
37 red shifted of 3 nm with respect to what computed in the gas phase, whereas the emission of **OPr**  
38  
39 in the crystal is blue shifted of 23 nm when the Mulliken EE is used. The absorption and emission  
40  
41 energies computed for the molecule at the crystal structure without electronic embedding are also  
42  
43 very similar to those computed in vacuum confirming that the structural changes between the two  
44  
45 aggregation states are minimal.  
46  
47

48  
49 As expected, also the vertical energies computed using the implicit solvation model are very  
50  
51 similar to those computed in the gas-phase, due to the relatively low dielectric constant of  
52  
53 chloroform.  
54  
55

56  
57 Regarding the comparison with experimental data, predictions are in fair agreement with the  
58  
59 available data,[6] discrepancies being within 0.1-0.2 eV. The full experimental absorption  
60  
61

1  
2  
3  
4 spectrum ( $\lambda_{\text{max,abs}} = 390$  nm) is available only for the compound in solution whereas for the  
5  
6 crystalline form only the maximum in the excitation spectra is available ( $\lambda_{\text{max,exc}} = 438$  nm).  
7

8  
9 It is interesting to note that the blue shift (30 nm) observed in the experimental fluorescent  
10  
11 spectra of **OPr** crystal ( $\lambda_{\text{exc}} = 589$  nm) with respect to chloroform ( $\lambda_{\text{exc}} = 619$  nm) is well  
12  
13 reproduced by our calculations. In fact, B3LYP/MM EE (Mulliken) calculations ( $\lambda_{\text{exc}} = 563$  nm)  
14  
15 provide a blue shift of 28 nm with respect to chloroform ( $\lambda_{\text{exc}} = 591$  nm).  
16  
17

18  
19 Overall, B3LYP results are very good. The frontier orbitals, depicted in **Figure 6** (and in Figures  
20  
21 S.3-S.8 of Supporting Information) clearly show that the HOMO-LUMO excitation possesses a  
22  
23 partial CT character, more marked for the keto tautomer when using the optimized  $S_1$  geometry.  
24

25  
26 It is worth to note that the B3LYP functional provided consistent results due to the limited  
27  
28 through-space character associated to these transitions. More importantly, the ESIPT feature of  
29  
30 the **OPr** system becomes noticeable when comparing the frontier orbitals of the enol tautomer,  
31  
32 where the density is delocalized over the whole molecule (except for the propoxy- group) and the  
33  
34 frontier orbitals of the keto tautomer, where a charge depletion arises, in turn, on the two lateral  
35  
36 aromatic groups.  
37  
38  
39  
40  
41  
42

43 *3.5 The effect of charges on the optical properties OPr in the solid state.* **Figure 7** reports the  
44  
45 UV-Visible spectra obtained from cluster calculations using different sets of charges in the low  
46  
47 level region. We recall that, in order to separate structural and electronic effects on the optical  
48  
49 properties, cluster calculations were performed using both  $S_0$  and  $S_1$  structures (obtained without  
50  
51 electronic embedding at the TD-B3LYP/6-31+G(d):HF/STO-3G level).  
52  
53

54  
55 **Figure 7** shows that the absorption region is overall less relevant than the emission region, as all  
56  
57 the methods furnish a very similar  $\lambda_{\text{max}}$ , with a maximal variation of 20 nm, evident from the  
58  
59 inset of the figure. Such differences fall within the limit of accuracy of the TD-DFT method used.  
60  
61  
62  
63  
64  
65

1  
2  
3  
4 The slight differences observed for peaks positions are, however, in agreement with the trend  
5  
6 reported for the emission of the **C-OPr-keto** clusters, for which more marked variations in  
7  
8  $\lambda_{\max, \text{emi}}$  are observed. This underlines the fact that electronic effects influence the excited state  
9  
10 properties more severely than those of the ground state.  
11  
12

13  
14 With respect to the experimental emission maximum in solid state ( $\lambda_{\max, \text{emi}} = 589 \text{ nm}$ ), the TD-  
15  
16 B3LYP/HF keto emission without embedding (orange dashes) is redshifted ( $\lambda_{\max, \text{emi}} = 605 \text{ nm}$ ),  
17  
18 whereas the method adopting the electronic embedding (i.e. TD-B3LYP/MM EE, green dashes)  
19  
20 features an opposite trend, i.e. a blueshift ( $\lambda_{\max, \text{emi}} = 563 \text{ nm}$ ). The difference between these two  
21  
22 values is relevant, and shows how the electronic embedding obtained using the HF/STO-3G  
23  
24 Mulliken charges induces an hypsochromic shift of the emission band.  
25  
26

27  
28 The spectra obtained at the TD-B3LYP/MM level with RESP charges computed at the HF/STO-  
29  
30 3G and HF/6-31G(d) are, indeed, mildly distinguishable (pink and violet dashes, respectively).  
31  
32 The robust formulation of such model of charges furnishes a  $\lambda_{\max, \text{emi}}$  of 591 nm (STO-3G), and a  
33  
34  $\lambda_{\max, \text{emi}}$  of 590 nm (6-31G(d)) that are significantly in better agreement with experiment, and  
35  
36 rather independent from the basis-set size. Though the minimal STO-3G basis-set is generally  
37  
38 discouraged to compute most properties for obvious reasons, it represents an interesting option,  
39  
40 especially from the point of view of the computational cost, in the perspective of being used to  
41  
42 calculate low-level charges for multiscale simulations.  
43  
44

45  
46 CM5 charges also provide a nice prediction ( $\lambda_{\max, \text{emi}} = 579 \text{ nm}$ ) of the experimental emission  
47  
48 wavelength in solid state, showing a spectral profile that mostly coincides with those furnished by  
49  
50 the RESP model.  
51  
52

53  
54 The  $Q_{\text{Eq}}$  charges, instead, furnishes a marked redshift (+41 nm,  $\lambda_{\max, \text{emi}} = 630 \text{ nm}$ ), compared to  
55  
56 experiment and to the other charge models tested.  
57  
58  
59  
60  
61  
62  
63  
64  
65



1  
2  
3  
4 Finally, another more important property that can be employed to evaluate the effect of  
5  
6 embedded charges, is the variation that refers to the experimental Stokes' shift which is 151 nm.  
7  
8 **Table 5** reports the Stokes' shift computed with different charges. Apart the  $Q_{Eq}$  charges, all the  
9  
10 other sets of charges provide small deviations from the experimental one, with Mulliken charges  
11  
12 yielding the best results.  
13  
14  
15  
16  
17

## 18 **Conclusions**

19  
20  
21 The absorption and emission energies of the **OPr** molecule in gas phase, in solution and  
22  
23 crystalline state have been investigated.  
24

25  
26 The absorption and emission spectra of the **OPr** molecule in the crystal have been computed by  
27  
28 using a protocol involving hybrid QM/MM ONIOM cluster calculations with the inclusion of  
29  
30 electrostatic embedding effects.  
31

32  
33 We have shown that the description of excited states depends crucially on the model adopted to  
34  
35 compute charges in the low level region (Mulliken, CM5, RESP and  $Q_{Eq}$  model charges have  
36  
37 been compared).  
38

39  
40 In fair agreement with experimental data, the absorption (emission) energies of the enol (keto)  
41  
42 **OPr** molecule is red shifted of about 3 (3) nm passing from the gas phase to chloroform and blue  
43  
44 shifted of 10 (23) nm passing from the gas to the crystal phase when the Mulliken charges are  
45  
46 employed. The Stokes' shift are also in reasonable agreement with experimental data apart for the  
47  
48 calculation employing the  $Q_{Eq}$  charges.  
49  
50  
51  
52  
53

## 54 **Acknowledgements**

55  
56  
57 H. P. Hratchian and M. J. Frisch are kindly acknowledged. Computational resources for this work  
58  
59 were granted by 'Project 100339' (2013-2014) at GENCI-IDRIS (Orsay, France). This work was  
60  
61  
62  
63  
64  
65

1  
2  
3  
4 supported by the Italian Ministero dell'Istruzione, dell' Università e della Ricerca (MIUR)  
5  
6 through the “Programma di Ricerca di rilevante Interesse Nazionale” (PRIN) Grant  
7  
8 2010C4R8M8\_002 entitled “Nanoscale Functional Organization of (bio)Molecules and Hybrids  
9  
10 for Targeted Application in Sensing, Medicine and Biotechnology” and the “Futuro in Ricerca”  
11  
12 (FIRB) Grant RBFR1248UI 002 entitled “Novel Multiscale Theoretical/Computational  
13  
14 Strategies for the Design of Photo and Thermo Responsive Hybrid Organic-Inorganic  
15  
16 Components for Nanoelectronic Circuits”.

17  
18  
19  
20  
21  
22  
23  
24 **Supporting Information.** B3LYP intramolecular parameters of the gas-phase enol **OPr** obtained  
25  
26 with different basis-sets; B3LYP-D\* results for the main structural enol parameters; molecular  
27  
28 atomic labelling and intermolecular interactions of the keto cluster; all frontier orbitals of gas-  
29  
30 phase tautomers, solvated ones and clusters.

31  
32  
33  
34  
35  
36 **References:**

- 37  
38  
39  
40  
41  
42  
43  
44  
45  
46  
47  
48  
49  
50  
51  
52  
53  
54  
55  
56  
57  
58  
59  
60  
61  
62  
63  
64  
65
1. Singer KD, Lalama SL, Sohn JE, Small RD (1987) Chapter II-8 - Electro-Optic Organic Materials. In: Zyss DSC (ed) Nonlinear Opt. Prop. Org. Mol. Cryst. Academic Press, pp 437–468
  2. Ramamurthy V (1991) Photochemistry in organized and constrained media. Wiley-VCH, New York
  3. Crano JC, Guglielmetti RJ (1999) Organic Photochromic and Thermochromic Compounds. Plenum Press, New York
  4. Irie M (2000) Diarylethenes for memories and switches. Chem Rev 100:1685–1716. doi: 10.1021/cr980069d
  5. Dürr H, Bouas-Laurent H (2003) Photochromism: Molecules and Systems, 2nd ed. Elsevier, Amsterdam
  6. Sakai K, Kawamura H, Kobayashi N, et al. (2014) Highly efficient solid-state red fluorophores using ESIPT: crystal packing and fluorescence properties of alkoxy-substituted dibenzothiazolyphenols. CrystEngComm 16:3180–3185. doi: 10.1039/C3CE42109K

- 1
- 2
- 3
- 4 7. Kasha M (1963) Energy Transfer Mechanisms and the Molecular Exciton Model for
- 5 Molecular Aggregates. *Radiat Res* 20:55–70. doi: 10.2307/3571331
- 6
- 7
- 8 8. Presti D, Labat F, Pedone A, et al. (2014) Computational Protocol for Modeling
- 9 Thermochromic Molecular Crystals: Salicylidene Aniline As a Case Study. *J Chem Theory*
- 10 *Comput* 10:5577–5585. doi: 10.1021/ct500868s
- 11
- 12 9. Mutai T, Satou H, Araki K (2005) Reproducible on–off switching of solid-state
- 13 luminescence by controlling molecular packing through heat-mode interconversion. *Nat*
- 14 *Mater* 4:685–687. doi: 10.1038/nmat1454
- 15
- 16
- 17 10. Harada J, Fujiwara T, Ogawa K (2007) Crucial Role of Fluorescence in the Solid-State
- 18 Thermochromism of Salicylideneanilines. *J Am Chem Soc* 129:16216–16221. doi:
- 19 10.1021/ja076635g
- 20
- 21
- 22 11. Chung JW, You Y, Huh HS, et al. (2009) Shear- and UV-Induced Fluorescence Switching
- 23 in Stilbenic  $\pi$ -Dimer Crystals Powered by Reversible [2 + 2] Cycloaddition. *J Am Chem*
- 24 *Soc* 131:8163–8172. doi: 10.1021/ja900803d
- 25
- 26 12. Hongo K, Watson MA, Sánchez-Carrera RS, et al. (2010) Failure of Conventional Density
- 27 Functionals for the Prediction of Molecular Crystal Polymorphism: A Quantum Monte
- 28 Carlo Study. *J Phys Chem Lett* 1:1789–1794. doi: 10.1021/jz100418p
- 29
- 30
- 31 13. Pedone A, Presti D, Menziani MC (2012) On the ability of periodic dispersion-corrected
- 32 DFT calculations to predict molecular crystal polymorphism in para-diiodobenzene. *Chem*
- 33 *Phys Lett* 541:12–15. doi: 10.1016/j.cplett.2012.05.049
- 34
- 35
- 36 14. Kronik L, Tkatchenko A (2014) Understanding Molecular Crystals with Dispersion-
- 37 Inclusive Density Functional Theory: Pairwise Corrections and Beyond. *Acc Chem Res*
- 38 47:3208–3216. doi: 10.1021/ar500144s
- 39
- 40
- 41 15. Grimme S (2006) Semiempirical GGA-type density functional constructed with a long-
- 42 range dispersion correction. *J Comput Chem* 27:1787–1799. doi: 10.1002/jcc.20495
- 43
- 44 16. Civalleri B, Zicovich-Wilson CM, Valenzano L, Ugliengo P (2008) B3LYP augmented with
- 45 an empirical dispersion term (B3LYP-D\*) as applied to molecular crystals. *Crystengcomm*
- 46 10:405–410. doi: 10.1039/b715018k
- 47
- 48
- 49 17. Svensson M, Humbel S, Froese RDJ, et al. (1996) ONIOM: A Multilayered Integrated MO
- 50 + MM Method for Geometry Optimizations and Single Point Energy Predictions. A Test for
- 51 Diels–Alder Reactions and Pt(P(t-Bu)<sub>3</sub>)<sub>2</sub> + H<sub>2</sub> Oxidative Addition. *J Phys Chem*
- 52 100:19357–19363. doi: 10.1021/jp962071j
- 53
- 54
- 55 18. Vreven T, Morokuma K (2000) The ONIOM (our own N-layered integrated molecular
- 56 orbital + molecular mechanics) method for the first singlet excited (S<sub>1</sub>) state
- 57 photoisomerization path of a retinal protonated Schiff base. *J Chem Phys* 113:2969–2975.
- 58 doi: 10.1063/1.1287059
- 59
- 60
- 61
- 62
- 63
- 64
- 65

- 1  
2  
3  
4 19. Stephens PJ, Devlin FJ, Chabalowski CF, Frisch MJ (1994) Ab Initio Calculation of  
5 Vibrational Absorption and Circular Dichroism Spectra Using Density Functional Force  
6 Fields. *J Phys Chem* 98:11623–11627. doi: 10.1021/j100096a001  
7  
8  
9 20. Dovesi R, Orlando R, Civalleri B, et al. (2005) CRYSTAL: a computational tool for the ab  
10 initio study of the electronic properties of crystals. *Z Krist* 220:571–573. doi:  
11 10.1524/zkri.220.5.571.65065  
12  
13 21. R. Dovesi, V. R. Saunders, C. Roetti, et al. (2010) CRYSTAL09 User's Manual. Università  
14 di Torino, Torino  
15  
16  
17 22. Presti D, Pedone A, Menziani MC, et al. (2014) Oxalyl dihydrazide polymorphism: a  
18 periodic dispersion-corrected DFT and MP2 investigation. *Crystengcomm* 16:102–109. doi:  
19 10.1039/c3ce41758a  
20  
21  
22 23. Presti D, Pedone A, Menziani MC (2014) Unraveling the Polymorphism of [(p-  
23 cymene)Ru( $\kappa$ N-INA)Cl<sub>2</sub>] through Dispersion-Corrected DFT and NMR GIPAW  
24 Calculations. *Inorg Chem* 53:7926–7935. doi: 10.1021/ic5006743  
25  
26  
27 24. Hariharan PC, Pople JA (1973) The influence of polarization functions on molecular orbital  
28 hydrogenation energies. *Theor Chim Acta* 28:213–222. doi: 10.1007/BF00533485  
29  
30  
31 25. Gill PMW, Johnson BG, Pople JA, Frisch MJ (1992) The performance of the Becke—  
32 Lee—Yang—Parr (B—LYP) density functional theory with various basis sets. *Chem Phys*  
33 *Lett* 197:499–505. doi: 10.1016/0009-2614(92)85807-M  
34  
35  
36 26. Cossi M, Rega N, Scalmani G, Barone V (2003) Energies, structures, and electronic  
37 properties of molecules in solution with the C-PCM solvation model. *J Comput Chem*  
38 24:669–681. doi: 10.1002/jcc.10189  
39  
40  
41 27. M. J. Frisch, G. W. Trucks, H. B. Schlegel, G. E. Scuseria, M. A. Robb, J. R. Cheeseman,  
42 G. Scalmani, V. Barone, B. Mennucci, G. A. Petersson, H. Nakatsuji, M. Caricato, X. Li, H.  
43 P. Hratchian, A. F. Izmaylov, J. Bloino, G. Zheng, J. L. Sonnenberg, W. Liang, M. Hada,  
44 M. Ehara, K. Toyota, R. Fukuda, J. Hasegawa, M. Ishida, T. Nakajima, Y. Honda, O. Kitao,  
45 H. Nakai, T. Vreven, J. A. Montgomery, Jr., J. E. Peralta, F. Ogliaro, M. Bearpark, J. J.  
46 Heyd, E. Brothers, K. N. Kudin, V. N. Staroverov, T. Keith, R. Kobayashi, J. Normand, K.  
47 Raghavachari, A. Rendell, J. C. Burant, S. S. Iyengar, J. Tomasi, M. Cossi, N. Rega, J. M.  
48 Millam, M. Klene, J. E. Knox, J. B. Cross, V. Bakken, C. Adamo, J. Jaramillo, R.  
49 Gomperts, R. E. Stratmann, O. Yazyev, A. J. Austin, R. Cammi, C. Pomelli, J. W.  
50 Ochterski, R. L. Martin, K. Morokuma, V. G. Zakrzewski, G. A. Voth, P. Salvador, J. J.  
51 Dannenberg, S. Dapprich, P. V. Parandekar, N. J. Mayhall, A. D. Daniels, O. Farkas, J. B.  
52 Foresman, J. V. Ortiz, J. Cioslowski, and D. J. Fox (2009) GAUSSIAN09, Revision D.01.  
53 Gaussian, Inc., Wallingford CT  
54  
55  
56 28. Mulliken RS (1955) Electronic Population Analysis on LCAO–MO Molecular Wave  
57 Functions. I. *J Chem Phys* 23:1833–1840. doi: 10.1063/1.1740588  
58  
59  
60  
61  
62  
63  
64  
65

- 1
- 2
- 3
- 4 29. Marenich AV, Jerome SV, Cramer CJ, Truhlar DG (2012) Charge Model 5: An Extension
- 5 of Hirshfeld Population Analysis for the Accurate Description of Molecular Interactions in
- 6 Gaseous and Condensed Phases. *J Chem Theory Comput* 8:527–541. doi:
- 7 10.1021/ct200866d
- 8
- 9
- 10 30. Bayly CI, Cieplak P, Cornell W, Kollman PA (1993) A well-behaved electrostatic potential
- 11 based method using charge restraints for deriving atomic charges: the RESP model. *J Phys*
- 12 *Chem* 97:10269–10280. doi: 10.1021/j100142a004
- 13
- 14
- 15 31. Singh UC, Kollman PA (1984) An approach to computing electrostatic charges for
- 16 molecules. *J Comput Chem* 5:129–145. doi: 10.1002/jcc.540050204
- 17
- 18 32. Rappe AK, Goddard WA (1991) Charge equilibration for molecular dynamics simulations. *J*
- 19 *Phys Chem* 95:3358–3363. doi: 10.1021/j100161a070
- 20
- 21
- 22 33. Martin F, Zipse H (2005) Charge distribution in the water molecule—A comparison of
- 23 methods. *J Comput Chem* 26:97–105. doi: 10.1002/jcc.20157
- 24
- 25
- 26
- 27
- 28
- 29
- 30
- 31
- 32
- 33
- 34
- 35
- 36
- 37
- 38
- 39
- 40
- 41
- 42
- 43
- 44
- 45
- 46
- 47
- 48
- 49
- 50
- 51
- 52
- 53
- 54
- 55
- 56
- 57
- 58
- 59
- 60
- 61
- 62
- 63
- 64
- 65

**Table 1.** Optimized (B3LYP-D\*) cell parameters and deviations relative to experiment, in parentheses (in Å, degrees and Å<sup>3</sup>). For the keto form, deviations are calculated with respect to the enol form. The Relative Deviation % (RD %) is reported for the cell volume. The relative stability computed at ground state ( $\Delta E = E_{\text{keto}} - E_{\text{enol}}$ , in kcal/mol) is also reported.

	OPr enol (dev.)		OPr keto (dev.)		Exp. OPr enol <sup>a</sup>
<i>a</i>	11.531	(-0.199)	11.483	(-0.048)	11.730
<i>b</i>	22.140	(-0.148)	21.970	(-0.170)	22.288
<i>c</i>	7.286	(-0.194)	7.299	(+0.013)	7.480
$\beta$	98.762	(-1.676)	98.186	(-0.576)	100.438
<b>Volume (RD %)</b>	1838.46	(-4.40)	1822.60	(-0.86)	1923.10
Relative Stability					
$E_{\text{keto}} - E_{\text{enol}}$	+19.745	<i>per cell</i>			
	+4.936	<i>per molecule</i>			

a: from Ref.[6]

**Table 2.** Comparison of selected *intermolecular* distances (in Å). Deviations (in parentheses) of cluster parameters are reported with respect to the two corresponding crystalline forms.

	B3LYP				Crystals B3LYP-D*	
	C-OPr-Enol		C-OPr-Keto		Enol	Keto
C16...H(a')	2.743	(0.008)	3.542	(-0.044)	2.735	3.586
H(a)...C16	2.735	(0.000)	3.578	(-0.008)	2.735	3.586
S2...H(b)	2.782	(-0.011)	2.883	(-0.003)	2.793	2.886
O1...H(c)	2.325	(-0.058)	2.265	(-0.015)	2.383	2.280
O2...H(d)	2.879	(0.018)	2.967	(0.004)	2.861	2.963
$\pi \cdots \pi$	3.647	(0.004)	3.650	(0.000)	3.643	3.650

**Table 3.** Selected intra- and intermolecular parameters (in Å) computed at the ground ( $S_0$ ) and first excited ( $S_1$ ) states for the keto tautomer in gas-phase, solvent and clusters.

<b>KETO</b>	<b>Gas <math>S_0</math></b>	<b>Gas <math>S_1</math></b>	<b>CHCl<sub>3</sub> <math>S_0</math></b>	<b>CHCl<sub>3</sub> <math>S_1</math></b>	<b>Cluster <math>S_0</math></b>	<b>Cluster <math>S_1</math></b>
S1–C1	1.765	1.764	1.759	1.761	1.751	1.749
N1–C1	1.343	1.362	1.341	1.363	1.338	1.354
C2–C3	1.398	1.406	1.398	1.405	1.396	1.404
S1–C7	1.769	1.773	1.768	1.768	1.762	1.768
O1–C13	1.278	1.278	1.279	1.270	1.284	1.285
C8–C13	1.456	1.462	1.454	1.475	1.448	1.455
O2–C10	1.368	1.365	1.368	1.355	1.365	1.363
C1–C8	1.412	1.437	1.419	1.432	1.416	1.449
N1···O1	2.474	2.593	2.514	2.628	2.492	2.610
O1···H	1.531	1.746	1.615	1.833	1.555	1.768
H–N1	1.075	1.039	1.055	1.028	1.073	1.038
N1–H–O1	142.7	135.7	139.7	131.3	142.4	135.4
<b>Intermolecular distances</b>						
C16···H(a')					3.542	3.581
H(a)···C16					3.578	3.613
S2···H(b)					2.883	2.870
O1···H(c)					2.265	2.208
O2···H(d)					2.967	3.043
$\pi$ ··· $\pi$					3.650	3.642



**Table 4.** Computed main vertical excitations and emission compared with experimental data, when available. ‘H-L’ stands for HOMO-LUMO. Energies in nm, oscillator strengths in a.u.

	<b>Form</b>	<b>Character</b>	$\lambda_{\max}$	<b>Osc. strength</b>
<b>Gas-phase</b>	enol	H-L 0.70	403.42	0.37
	keto	H-L 0.70	586.85	0.34
<b>CHCl<sub>3</sub></b>	enol	H-L 0.70	406.50	0.53
	Exp. absorption <sup>a</sup>		390	
	keto	H-L 0.70	590.57	0.65
	Exp. emission <sup>a</sup>		619	
<b>Clusters</b>				
B3LYP/HF No EE	C-OPr-enol	H-L 0.70	402.15	0.37
B3LYP/MM EE Mulliken (HF/STO-3G)		H-L 0.70	393.35	0.40
B3LYP/MM EE RESP (HF/STO-3G)		H-L 0.70	393.73	0.38
B3LYP/MM EE RESP (HF/6-31G(d))		H-L 0.70	396.27	0.37
B3LYP/MM EE CM5 (HF/6-31G(d))		H-L 0.70	393.60	0.39
B3LYP/MM EE Q <sub>Eq</sub>		H-L 0.70	403.35	0.33
	Exp. Fluo. Excitation Crystal <sup>a</sup>		438	
B3LYP/HF No EE	C-OPr-keto	H-L 0.71	605.46	0.31
B3LYP/MM EE Mulliken (HF/STO-3G)		H-L 0.71	562.90	0.35
B3LYP/MM EE RESP (HF/STO-3G)		H-L 0.71	580.62	0.33
B3LYP/MM EE RESP (HF/6-31G(d))		H-L 0.71	580.20	0.33
B3LYP/MM EE CM5 (HF/6-31G(d))		H-L 0.71	579.11	0.32
B3LYP/MM EE Q <sub>Eq</sub>		H-L 0.71	629.53	0.27
	Exp. Fluo. Emission Crystal <sup>a</sup>		589	

a: from Ref.[6]

**Table 5.** Computed Stokes' shifts for the cluster moieties vs. experiment.

<b>Approach</b>	<b>Stokes' shift (nm)</b>
B3LYP/HF No EE	203
B3LYP/MM EE Mulliken (HF/STO-3G)	170
B3LYP/MM EE RESP (HF/STO-3G)	187
B3LYP/MM EE RESP (HF/6-31G(d))	184
B3LYP/MM EE CM5 (HF/6-31G(d))	185
B3LYP/MM EE Q <sub>Eq</sub>	226
Exp.	151

1  
2  
3  
4 **CAPTIONS TO FIGURES**  
5  
6

7 **Figure 1.** Scheme of the ESIPT process that takes place for **OPr**.  
8  
9

10 **Figure 2.** View (*ab* plane) of the fully optimized **a)** enol and **b)** keto ground state crystalline  
11 forms of **OPr**. Intramolecular hydrogen bonds are displayed in enhanced views. The unit cell,  
12 containing four symmetry-equivalent molecules, is highlighted in violet.  
13  
14  
15  
16  
17

18 **Figure 3.** (Top left) Perspective and (Top right) top view of the optimized **C-OPr-enol** cluster;  
19 the central molecule is highlighted in red. (Bottom) Labeling of selected intermolecular distances  
20 is given.  
21  
22  
23  
24

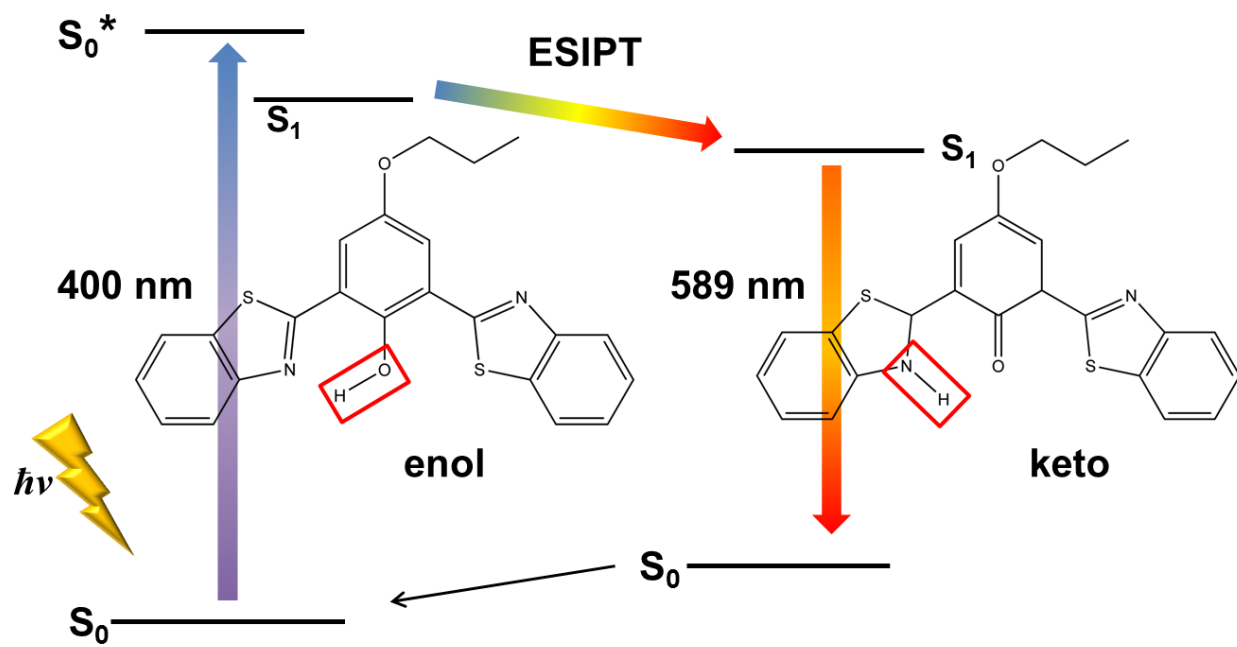
25 **Figure 4.** Difference between distances of selected intra- and intermolecular parameters for the  
26 **OPr** keto tautomer computed at the excited ( $S_1$ ) and ground ( $S_0$ ) states.  
27  
28  
29  
30

31 **Figure 5.** Spectra computed for the enol (absorption, continuous lines) and keto (emission,  
32 dashed lines) tautomers of **OPr** in gas-phase and in solution (chloroform). The spectra obtained  
33 from QM/MM embedded cluster calculations (HF/STO-3G Mulliken charges in the low level  
34 region) are also reported.  
35  
36  
37  
38  
39

40 **Figure 6.** Frontier orbitals derived from embedded cluster calculations of **OPr**, computed at  
41 B3LYP/MM EE (Mulliken) (right) and B3LYP/MM EE (CM5) (left) levels.  
42  
43  
44

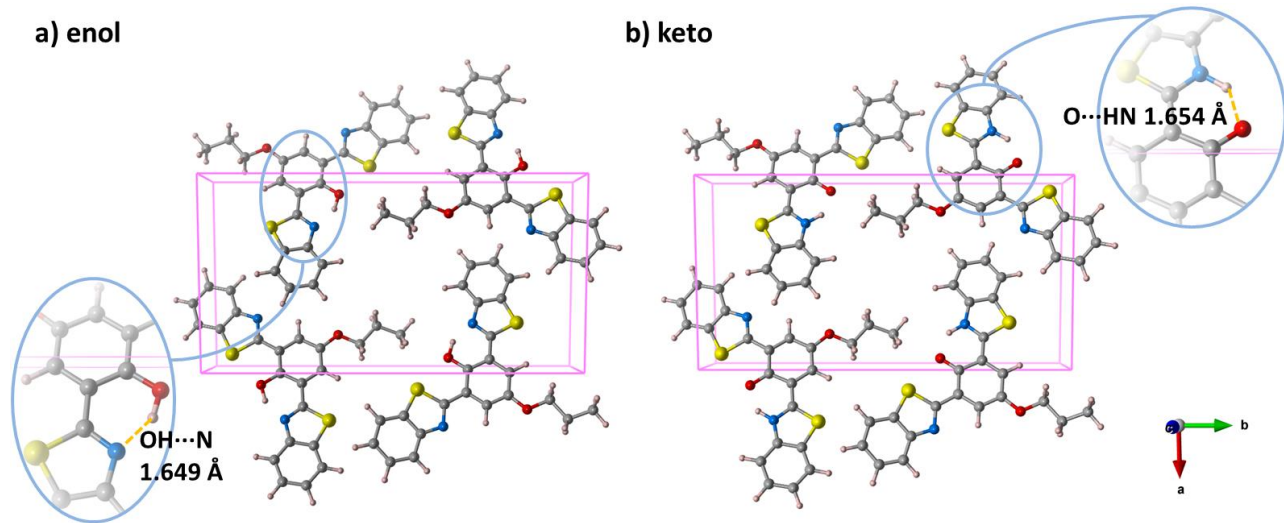
45 **Figure 7.** UV-Visible spectra computed for the **C-OPr-enol** (absorption, continuous lines) and  
46 **C-OPr-keto** (emission, dashed lines) clusters, obtained by using different charge embedding  
47 protocols. The inset shows an enhanced view of the absorption region.  
48  
49  
50  
51  
52  
53  
54  
55  
56  
57  
58  
59  
60  
61  
62  
63  
64  
65

FIGURE 1



1  
2  
3  
4  
5  
6  
7  
8  
9  
10  
11  
12  
13  
14  
15  
16  
17  
18  
19  
20  
21  
22  
23  
24  
25  
26  
27  
28  
29  
30  
31  
32  
33  
34  
35  
36  
37  
38  
39  
40  
41  
42  
43  
44  
45  
46  
47  
48  
49  
50  
51  
52  
53  
54  
55  
56  
57  
58  
59  
60  
61  
62  
63  
64  
65

**FIGURE 2**



1  
2  
3  
4 **FIGURE 3**  
5  
6  
7  
8  
9

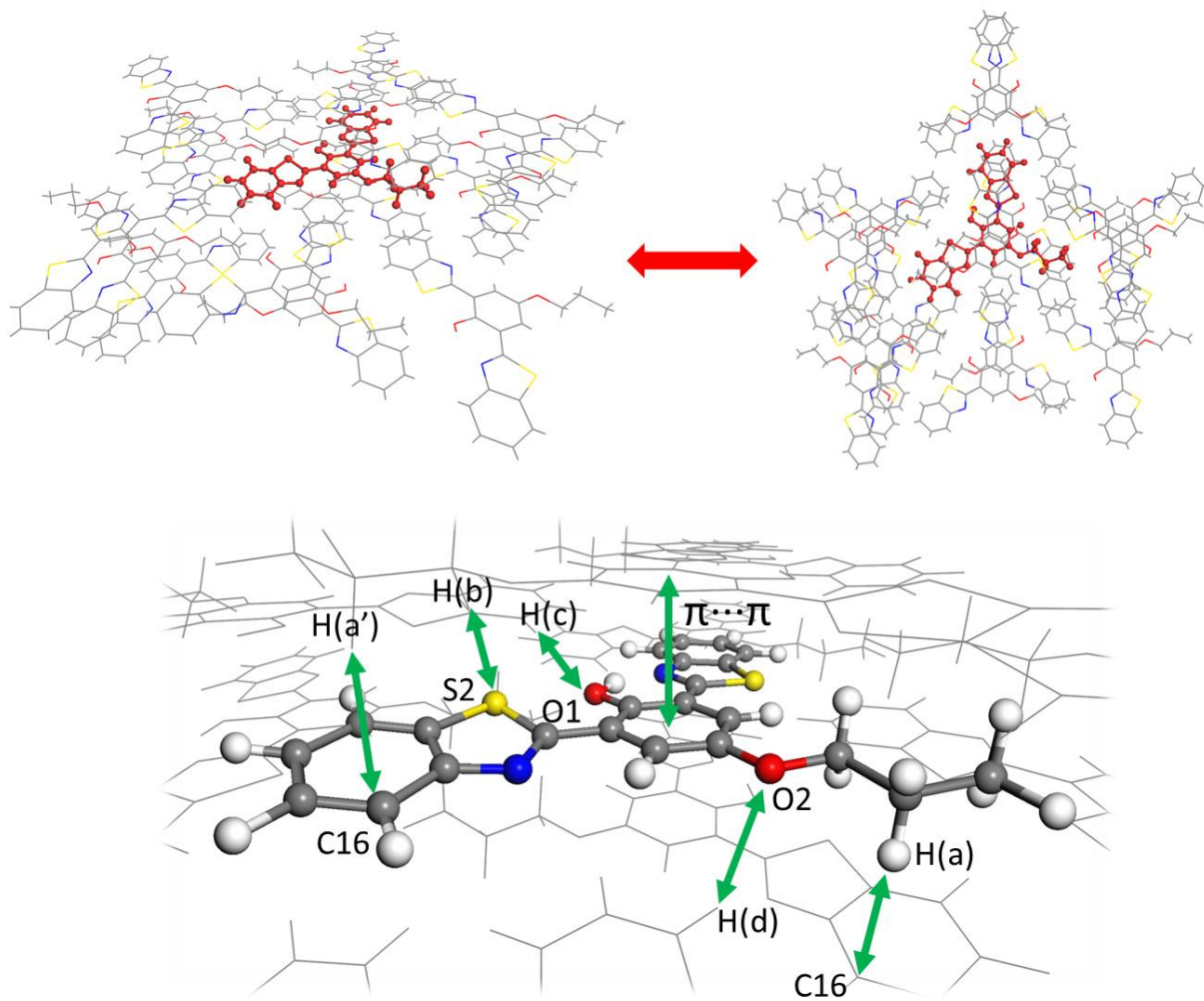
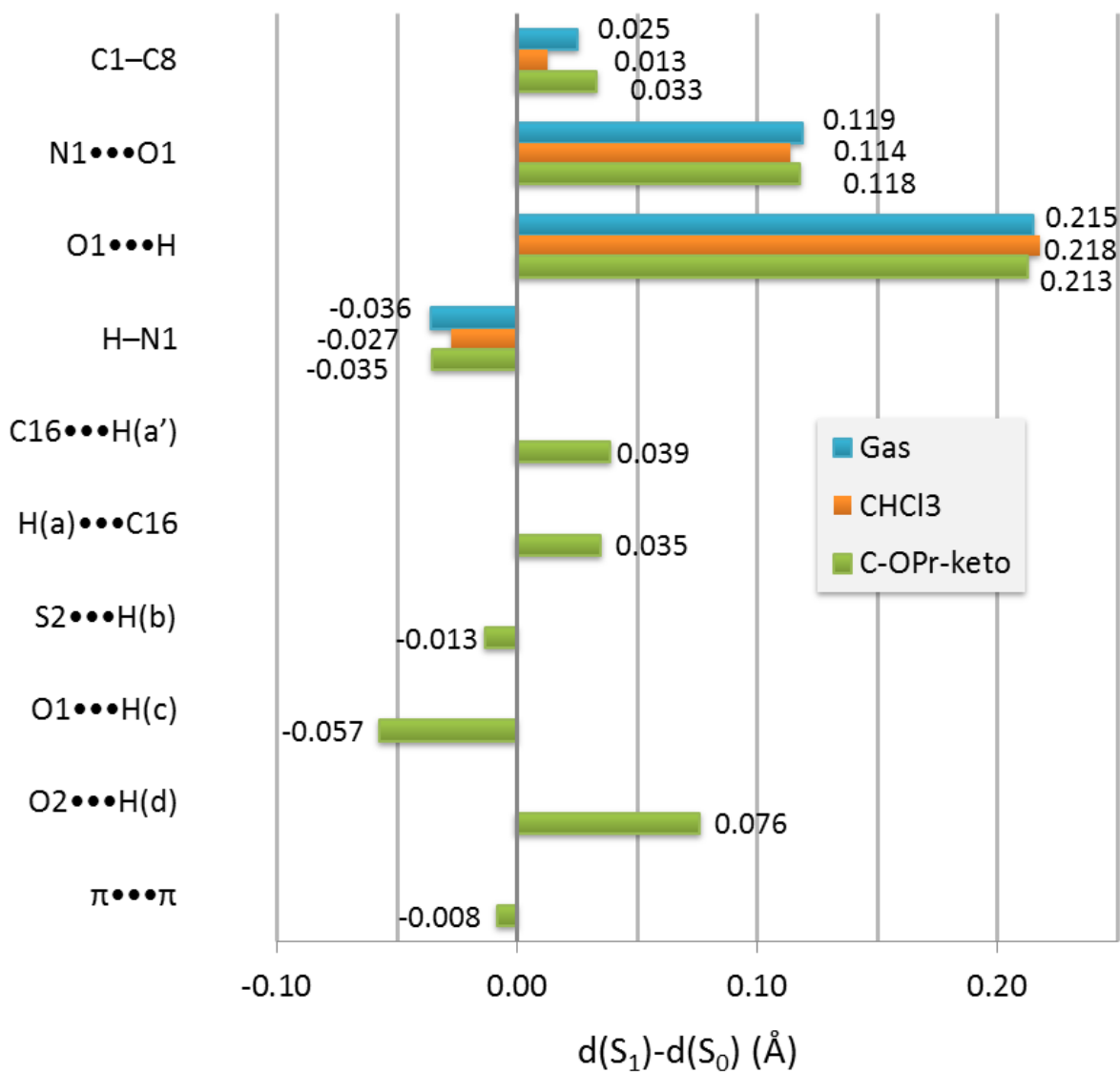
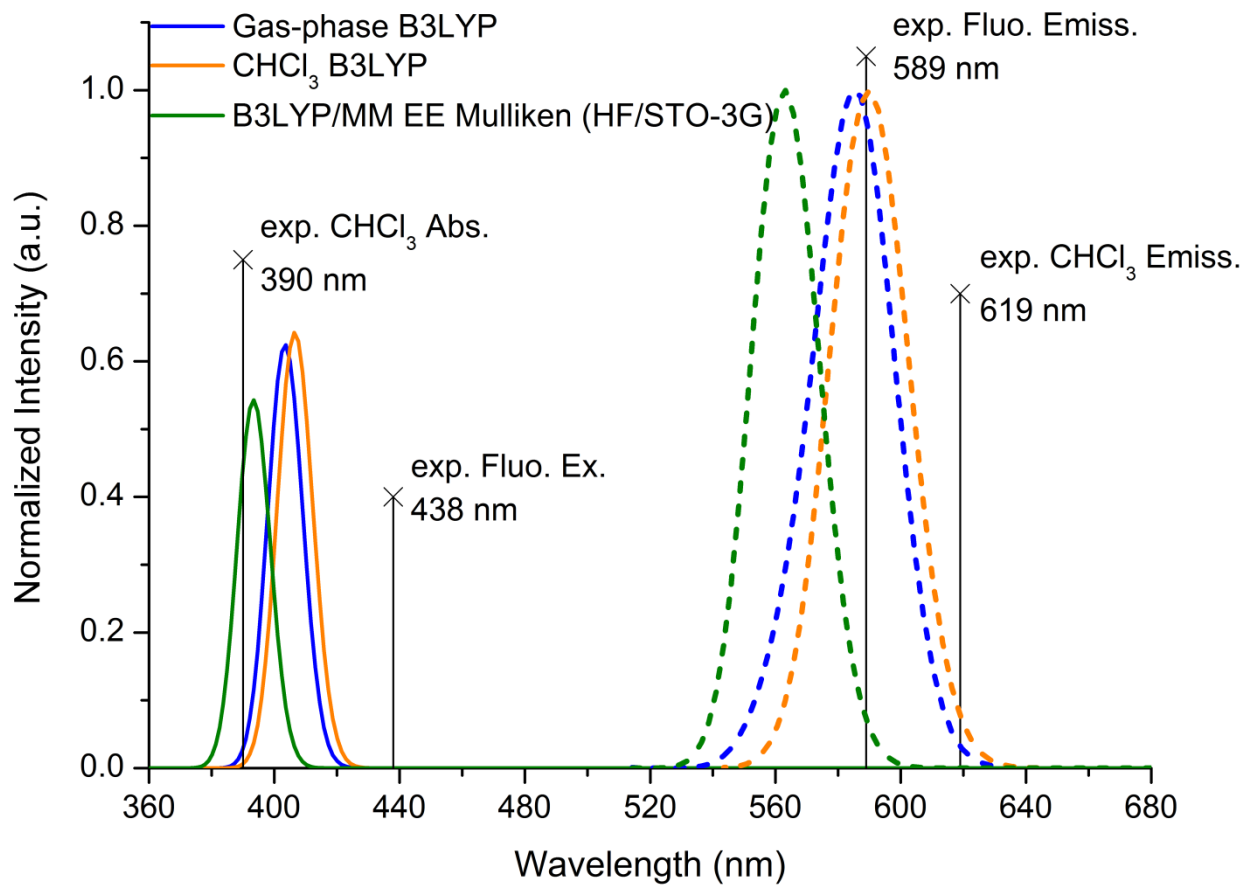


FIGURE 4



1  
2  
3  
4 **FIGURE 5**  
5  
6  
7  
8  
9





1  
2  
3  
4 **FIGURE 6**  
5  
6  
7  
8  
9

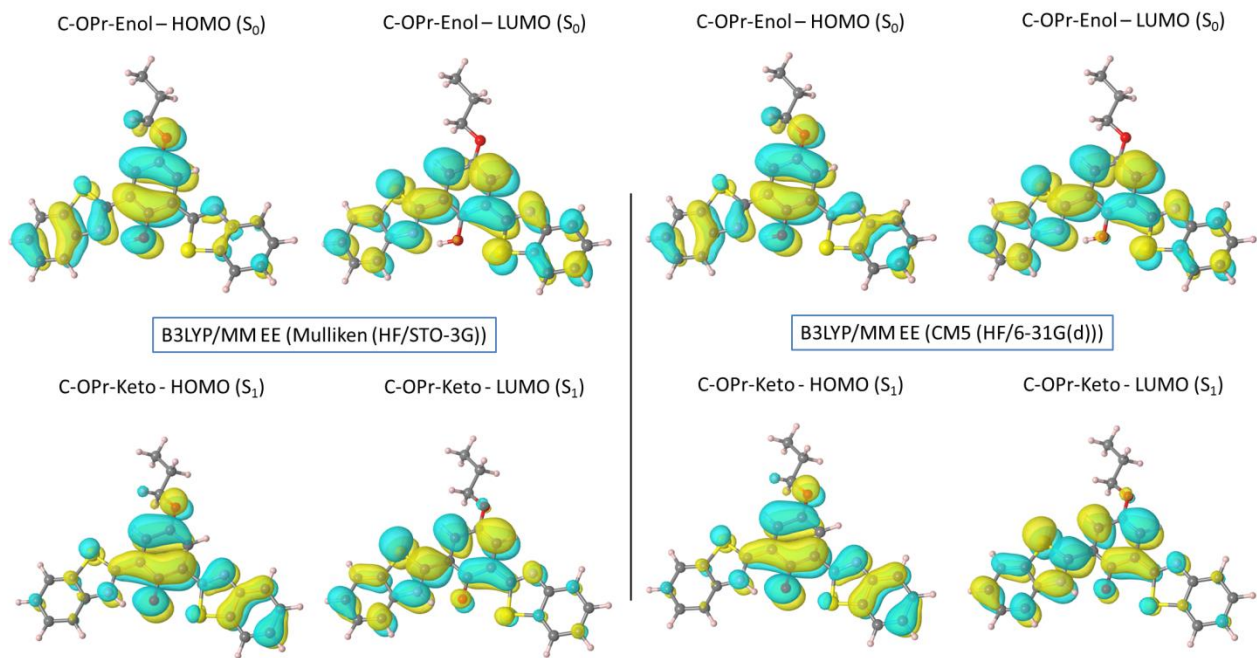
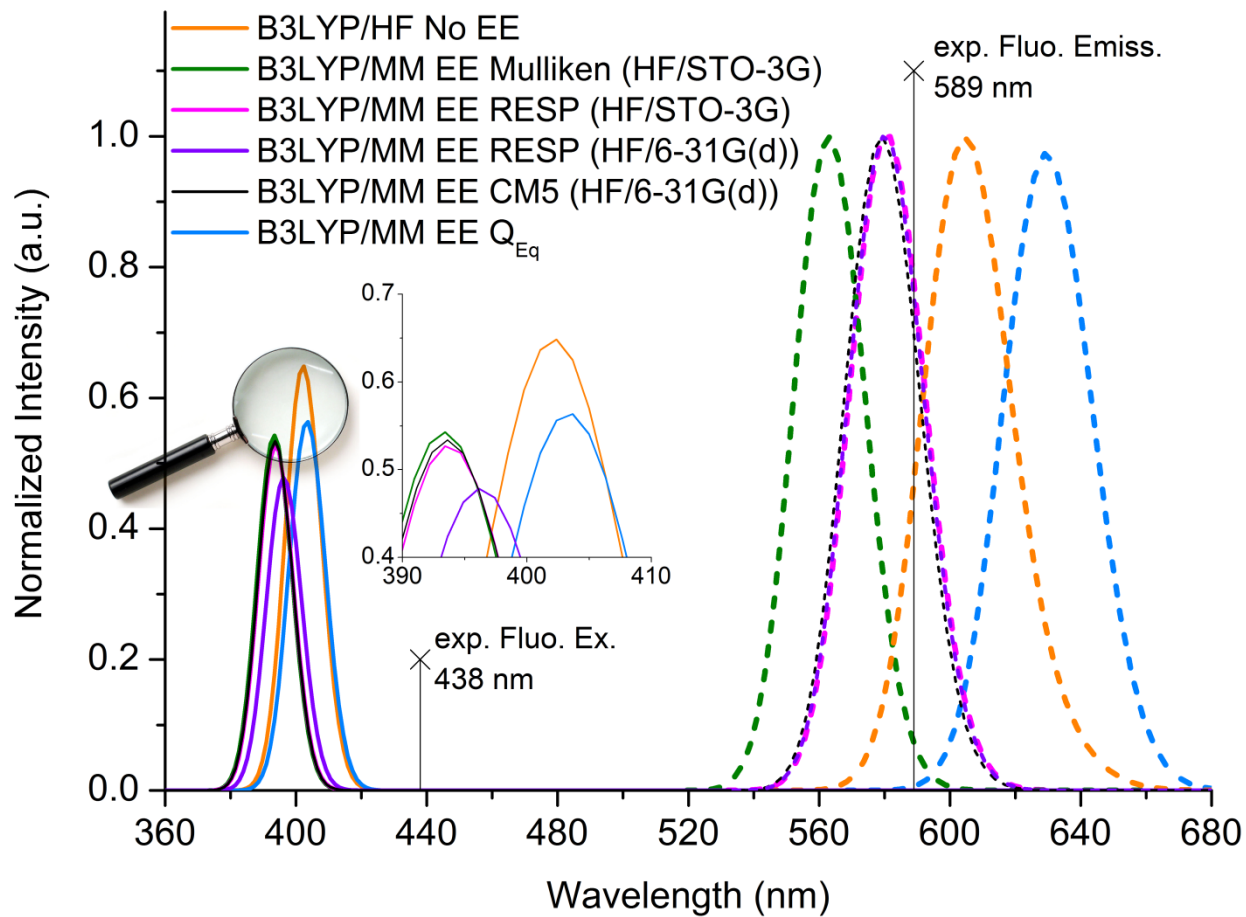
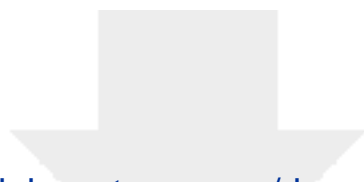


FIGURE 7





Click here to access/download

**Electronic Supplementary Material**  
ESI\_SpecialCT\_Presti.pdf

